V European Conference on Computational Fluid Dynamics
ECCOMAS CFD 2010
J. C. F. Pereira and A. Sequeira (Eds)
Lisbon, Portugal,14-17 June 2010

ON THE SYMMETRY-PRESERVING REGULARIZATION MODEL ON COMPLEX FLOWS USING UNSTRUCTURED GRIDS

O. Lehmkuhl[*,†], R. Borrell[†], I. Rodríguez[*], C.D. Pérez-Segarra[*] and A. Oliva[*]

[*]Centre Tecnològic de Transferència de Calor, Universitat Politècnica de Catalunya,
ETSEIAT, Colom 11, 08222 Terrassa (Barcelona), Spain
e-mail: cttc@cttc.upc.edu
[†]Termo Fluids, S.L.
Magí Colet, 8, 08204 Sabadell (Barcelona), Spain
e-mail: termofluids@yahoo.es

Key words: Turbulence modeling, regularization models, discrete filters, unstructured meshes

Abstract. *Traditionally turbulence modeling of industrial flows in complex geometries have been solved using RANS models and unstructured meshes based solvers. The lack of precision of RANS models in these situations and the increase of computer power, together with the emergence of new high-efficiency sparse parallel algorithms, make posible the use of more accurate turbulent models such as Large Eddy Simulation models (LES). Recently, relevant improvements on turbulence modeling based on symmetry-preserving regularization models for the convective (non-linear) term have been developed. They basically alter the convective terms to reduce the production of small scales of motion by means of vortex-stretching, preserving all inviscid invariants exactly. To do so, symmetry and conservation properties of the convective terms are exactly preserved. This requirement yields a novel class of regularizations that restrain the convective production of smaller and smaller scales of motion by means of vortex stretching in an unconditional stable manner, meaning that the velocity can not blow up in the energy-norm (in 2D also: enstrophynorm). The numerical algorithm used to solve the governing equations must preserve the symmetry and conservation properties too. At this stage, results using regularization models at relatively complex geometries and configurations are of extreme importance for further progress.*

The main objective of the present paper is the assessment of regularization models on unstructured meshes. To do this, three different test cases have been studied: the impinging jet flow, the flow past a circular cylinder and a simplified Ahmed car. In order to analyse the influence of the filter, the cases have been solved using the Gaussian and the Helmholtz filters. Furthermore, the performance of the model considering the influence of the grid parameters and the filter ratio are also analysed.

1 INTRODUCTION

The Navier-Stokes and continuity equations can be written as

$$\mathsf{M}\boldsymbol{u} = \mathbf{0} \tag{1}$$

$$\frac{\partial \boldsymbol{u}}{\partial t} + \mathsf{C}(\boldsymbol{u})\,\boldsymbol{u} + \nu \mathsf{D}\boldsymbol{u} + \rho^{-1}\mathsf{G}\boldsymbol{p} = \mathbf{0} \tag{2}$$

where $\boldsymbol{u} \in \mathbb{R}^{3m}$ and $\boldsymbol{p} \in \mathbb{R}^{m}$ are the velocity vector and pressure, respectively (here m applies for the total number of control volumes (CV) of the discretised domain), ν is the kinematic viscosity and ρ the density. Convective and diffusive operators in the momentum equation for the velocity field are given by $\mathsf{C}(\boldsymbol{u}) = (\boldsymbol{u}\cdot\nabla) \in \mathbb{R}^{3m\times 3m}$, $\mathsf{D} = \nabla^2 \in \mathbb{R}^{3m\times 3m}$ respectively. Gradient and divergence (of a vector) operators are given by $\mathsf{G} = \nabla \in \mathbb{R}^{3m\times 3m}$ and $\mathsf{M} = \nabla\cdot \in \mathbb{R}^{m\times 3m}$ respectively.

In the quest for a correct modeling of Navier Stokes equations (Eqn. 2), they can be filtered spatially as in LES. Doing so, the filtered non-linear convective term must be modeled,

$$\begin{aligned}\frac{\partial \overline{\boldsymbol{u}_c}}{\partial t} + \mathsf{C}(\overline{\boldsymbol{u}_c})\,\overline{\boldsymbol{u}_c} + \nu \mathsf{D}\overline{\boldsymbol{u}_c} + \rho^{-1}\mathsf{G}\overline{\boldsymbol{p}_c} - \overline{\boldsymbol{f}_c} &= \mathsf{C}(\overline{\boldsymbol{u}_c})\,\overline{\boldsymbol{u}_c} - \overline{\mathsf{C}(\boldsymbol{u}_c)\,\boldsymbol{u}_c} \\ &\approx -\mathcal{M}_c\mathcal{T}_\mathsf{c}\end{aligned} \tag{3}$$

where $\overline{\boldsymbol{u}_c}$ is the filtered velocity, $\mathcal{M}_c$ represents the divergence operator of a tensor, and $\mathcal{T}_\mathsf{c}$ is the SGS stress tensor, which is defined as[1],

$$\mathcal{T}_\mathsf{c} = -2\nu_{sgs}\overline{\mathcal{S}_\mathsf{c}} + (\mathcal{T}_\mathsf{c} : \mathsf{I})\mathsf{I}/3 \tag{4}$$

To close the formulation a suitable expression for the SGS-viscosity must be introduced. Smagorinsky proposed the following approach which is an adaptation of Prandtl's mixing length theory to subgrid-scale modeling, i.e., eddy viscosity arising in RANS equations is proportional to a turbulence characteristic scale (the mixing length) multiplied by a turbulence characteristic velocity. In the same way, Smagorinsky supposed that LES eddy viscosity is proportional to a subgrid scale characteristic length l, and to a characteristic subgrid-scale velocity[2]. Then,

$$\begin{aligned}\nu_{sgs} &= (c_s l)^2 \mid \overline{\mathcal{S}_\mathsf{c}} \mid \\ \mid \overline{\mathcal{S}_\mathsf{c}} \mid &= (2\overline{\mathcal{S}_\mathsf{c}} : \overline{\mathcal{S}_\mathsf{c}})^{1/2} \\ \overline{\mathcal{S}_\mathsf{c}} &= \frac{1}{2}[\mathsf{G}(\overline{\boldsymbol{u}_c}) + \mathsf{G}^*(\overline{\boldsymbol{u}_c})]\end{aligned} \tag{5}$$

where l is the grid cutting length and c_s is the Smagorinsky coefficient, which may be tuned so that the model reproduces the cascade when simulating isotropic decay. As it is well known, the value of this coefficient lies in the range between 0.1 and 0.24, depending on the numerical method used to solve the equations. However, this model is not appropriate

in the close vicinity of a solid wall subject to dominant molecular-viscosity effects. Thus, a near-wall correction is also required. Traditionally, the well-known Van Driest damping function[3], $f_{VD} = 1 - \exp(-\frac{y^+}{25})$, is introduced substituting the length scale in Eq. 5, i.e.

$$l \rightarrow l f_{VD} \equiv l(1 - \exp(-\frac{y^+}{25})) \tag{6}$$

where $y^+ = \frac{u_\tau y}{\nu}$ is the nondimensional distance to the wall, y is the wall normal coordinate and u_τ is the wall friction velocity.

The use of this Van Driests damping function is a strong constraint on the applicability of the model to a wide range of engineering flows because the function is written using wall-unit coordinates. The identification of the normal distance to the wall (y) is straightforward in the case of a plane wall and structured meshes, but it is quite ambiguous near highly curved walls or sharp corners with unstructured meshes.

The other main limitation of this damping function lies in the use of the friction velocity (u_τ). Near a separation point, the friction velocity vanishes or becomes very small. This results in inaccurate evaluation of the SGS-viscosity effect, which leads to the model to perform inadequately in these situations.

As a conclusion, to widen the applicability of LES to various types of engineering flows, and to use LES on unstructured meshes, it is advisable to seek SGS models free from the use of wall-unit coordinates such as the Variational Multiscale Method (VMS[4]), the wall adapting local eddy viscosity method (WALE[5]) or the Regularization models[6]. In the following sections, the use of regularization models to overcome these problems will be discussed.

2 REGULARIZATION MODELS

Geurts and Holm[6] have recently introduced the regularization principle as a new approach for large eddy simulation modeling. The underlaying idea is to express the smoothing of the dynamics of the Navier-Stokes equations through a specific proposal for direct alteration of the nonlinear convective terms. In contrast to the traditional LES modeling, Geurts and Holm regularization approach involves the introduction of a filter pair $(\mathcal{F}, \mathcal{F}^{-1})$ to fully specify the subgrid model. This modeling strategy has a number of important benefits, addressing directly the nonlinear convective contributions and requiring no additional external information such as model coefficients.

To illustrate this approach, the pioneering Leray regularization model[7] is considered. The model replaces convective terms by $\mathsf{C}\left(\overline{\boldsymbol{u}_c}\right)\boldsymbol{u}_c$. Thus, the solution is convected with a smoothed velocity. Taking into account this definition, the model can be written as,

$$\frac{\partial \boldsymbol{u}_c}{\partial t} + \mathsf{C}\left(\overline{\boldsymbol{u}_c}\right)\boldsymbol{u}_c + \nu \mathsf{D}\boldsymbol{u}_c + \rho^{-1}\mathsf{G}\boldsymbol{p}_c \;\; = \;\; \mathbf{0} \tag{7}$$

At this point Geurts and Holm, introduced the inversion operator, $\boldsymbol{u}_c = \mathcal{F}^{-1}\overline{\boldsymbol{u}_c}$, in the Eqn. 7, obtaining the following expression analogous to the LES concept (see Eqn. 3),

$$\frac{\partial \overline{\boldsymbol{u}_c}}{\partial t} + \mathsf{C}\left(\overline{\boldsymbol{u}_c}\right)\overline{\boldsymbol{u}_c} + \nu\mathsf{D}\overline{\boldsymbol{u}_c} + \rho^{-1}\mathsf{G}\overline{\boldsymbol{p}_c} = \mathsf{C}\left(\overline{\boldsymbol{u}_c}\right)\overline{\boldsymbol{u}_c} - \mathcal{F}(\mathsf{C}\left(\overline{\boldsymbol{u}_c}\right)\mathcal{F}^{-1}\overline{\boldsymbol{u}_c}) \tag{8}$$

Thus, an equivalent SGS stress ($\mathcal{T}_\mathsf{c}$) can be obtained from,

$$-\mathcal{M}_c\mathcal{T}_\mathsf{c} = \mathsf{C}\left(\overline{\boldsymbol{u}_c}\right)\overline{\boldsymbol{u}_c} - \mathcal{F}(\mathsf{C}\left(\overline{\boldsymbol{u}_c}\right)\mathcal{F}^{-1}\overline{\boldsymbol{u}_c}) \tag{9}$$

This model requires the explicit application of both $\mathcal{F}$ and $\mathcal{F}^{-1}$. As a consecuence, some technical complications arising from the reconstruction of an accurate inverse operator $\mathcal{F}^{-1}$ appear. In addition to this problem, Geurts and Holm also reported that the model does not provide sufficient smoothing and leads to unstable LES on coarse grids at high Reynolds numbers.

A solution to these problems has been raised recently by Verstappen[8]. First, the use of the $\mathcal{F}^{-1}$ is not necessary if Eqn. 7 is solved directly. On the other hand, the unstable behaviour of the Leray model may be related with the fact that this model does not conserve all the inviscid invariants (kinetic energy, enstrophy in 2D and helicity in 3D). Verstappen proposal is to approximate the convective nonlinearity in such a manner that the symmetry properties that form the basis for the conservation of the inviscid invariants are preserved, and at the same time, the production of small scales is restrained.

These criteria yield the following class of regularizations[8],

$$\mathcal{C}_2(\boldsymbol{u},\boldsymbol{v}) = \overline{\mathsf{C}\left(\overline{\boldsymbol{u}}\right)\overline{\boldsymbol{v}}} \tag{10}$$

$$\mathcal{C}_4(\boldsymbol{u},\boldsymbol{v}) = \mathsf{C}\left(\overline{\boldsymbol{u}}\right)\overline{\boldsymbol{v}} + \overline{\mathsf{C}\left(\overline{\boldsymbol{u}}\right)\boldsymbol{v}'} + \overline{\mathsf{C}\left(\boldsymbol{u}'\right)\overline{\boldsymbol{v}}} \tag{11}$$

where the prime indicates the residual of the filter, i.e. $\boldsymbol{u}' = \boldsymbol{u} - \overline{\boldsymbol{u}}$, which can be explicitly evaluated, and $\overline{(\cdot)}$ represents a normalised self-adjoint linear filter. The difference between $\mathcal{C}_q(\boldsymbol{u},\boldsymbol{u})$ and the original $\mathsf{C}\left(\boldsymbol{u}\right)\boldsymbol{u}$ is of the order ϵ^q (where $q = 2, 4, ...$) for symmetric filters with filter length ϵ. Note that for a generic symmetric filter: $\boldsymbol{u}' = \mathcal{O}(\epsilon^q)\boldsymbol{u}$.

The approximations $\mathcal{C}_q(\boldsymbol{u},\boldsymbol{v})$ are stable by construction, meaning that convective terms do not contribute to the evolution of $|\boldsymbol{u}_\epsilon|^2$. Hence, the evolution of both quantities is governed by a dissipative process. Therefore, replacing the convective term in the Navier-Stokes equations by the $\mathcal{O}(\epsilon^q)$-accurate smooth approximation, the partial differential equations to be solved are,

$$\mathsf{M}\boldsymbol{u} = \boldsymbol{0} \tag{12}$$

$$\frac{\partial \boldsymbol{u}}{\partial t} + \mathcal{C}_q(\boldsymbol{u},\boldsymbol{u}) + \nu\mathsf{D}\boldsymbol{u} + \rho^{-1}\mathsf{G}\boldsymbol{p} = \boldsymbol{0} \tag{13}$$

Note that $\mathcal{C}_q$ approximations are also skew-symmetric operators, as the original convective operator. Hence, the same inviscid invariants characteristics of the original Navier-Stokes equations (kinetic energy, enstrophy in 2D and helicity) are preserved for the new set of partial differential equations[8].

3 DISCRETE FILTERS

Since $\mathcal{C}_q$-regularization governing equations, Eqn. 13, are formally derived applying a low-pass filter to Navier-Stokes equations, it can be argued that its performance will be directly dependent of this filtering procedure. Furthermore, the properties of discrete filters can differ a lot from those of continuous filters, which are the basis of the theorical analysis. More specifically, the $\mathcal{C}_q$-regularization, in order to ensure all the symmetry and conservation properties, needs a normalized self-adjoint filter, thus

$$\Omega_c \mathcal{F} = (\Omega_c \mathcal{F})^* \tag{14}$$

$$\mathcal{F}1 = 1 \tag{15}$$

In other words, it is assumed that the filter has the following properties: (i) symmetry (see Eqn. 14), (ii) a constant velocity vector is unaffected by the filter (see Eqn. 15), and (iii) it reduces the high-frequency components of the discrete velocity vector $\boldsymbol{u}$.

On the other hand, similar to LES, in order to correct manipulate the modified Navier-Stokes equations, the filter needs to posses some extra properties. In general a suitable $\mathcal{C}_q$-regularization filter has to commutate with the addition, $\overline{\varphi + \omega} = \overline{\varphi} + \overline{\omega}$, and also with the differentation, $\overline{\frac{\partial \varphi}{\partial x_i}} = \frac{\partial \overline{\varphi}}{\partial x_i}$. Since filters are lineal operators, they automatically verify the commutation with the addition. Unfortunately, this is not true for the differentation operations when the filter width is not uniform. Since unstructured mesh rarely satisfy smoothness constrains on the grid spacing, the assumptions that the operations of filtering and differentation commute may be violated even away from walls.

Haselbacher et al., had proposed a new methodology that allows to construct commutative discrete filters on unstructured meshes[9]. This filter is based on least-squares techniques. The key concept of this new filter is that the filter weights exhibit vanishing moments. The larger the number of vanishing moments, the higher the order of commutation error. The advantage of this filter is that is truly constructed in three dimensions and no transformation from physical to computational space is required. The filter is based on the classical least-squares gradient reconstruction method developed by Barth[9]. This method is based on approximating the variation of the dependent variable ϕ along an edge linking points 0 and i by truncated Taylor series, that is, for a linear approximation,

$$\phi_i = \phi_0 + \Delta x_{0i} \frac{\partial \phi}{\partial x}, \qquad\qquad i = 1, ..., n \tag{16}$$

where n is the number of neighbours of the point 0. The application of Eqn. 16 to a set of selected points gives a linear system of equations for the derivatives at point 0. Finally this set of equations can be written as an overdetermined system of linear equations,

$$\mathsf{A}\boldsymbol{x} = \boldsymbol{b} \tag{17}$$

the algebraic solution of this system of equations can be obtained evaluating the Moore-Penrose pseudoinverse of A,

$$\hat{\boldsymbol{x}} = (\mathsf{A}^*\mathsf{A})^{-1}\mathsf{A}^*\boldsymbol{b} = \mathsf{A}^+\boldsymbol{b} \tag{18}$$

where A^* is the transpose of A and A^+ is the pseudoinverse. Since this system of equations is relatively small, a direct method can be used in order to solve Eqn. 18.

The least-squares gradient reconstruction method can be turned into a filtering method by modifying Eqn. 16. Thus, in one dimension, the general reconstruction equation for a second-order filter is,

$$\phi_i = \overline{\phi_0} + \Delta x_{0i}\frac{\partial \phi}{\partial x} + \frac{\Delta x_{0i}^2}{2!}\frac{\partial^2 \phi}{\partial x^2}, \qquad i = 1, ..., n \tag{19}$$

where n is the number of points of the stencil used by the filtering method and $\overline{\phi_0}$ is the filtered value at point 0. In three dimensions the number of terms in the Taylor expansion for this filter grows rapidly,

$$\begin{aligned} \phi_i = \overline{\phi_0} \quad &+ \quad \Delta x_{0i}\frac{\partial \phi}{\partial x} \\ &+ \quad \frac{1}{2!}\Delta x_{0i}^2\frac{\partial^2 \phi}{\partial x^2} + \frac{1}{2!}\Delta y_{0i}^2\frac{\partial^2 \phi}{\partial y^2} + \frac{1}{2!}\Delta z_{0i}^2\frac{\partial^2 \phi}{\partial z^2} \\ &+ \quad \frac{2}{2!}\Delta x_{0i}\Delta y_{0i}\frac{\partial^2 \phi}{\partial x \partial y} + \frac{2}{2!}\Delta x_{0i}\Delta z_{0i}\frac{\partial^2 \phi}{\partial x \partial z} \\ &+ \quad \frac{2}{2!}\Delta y_{0i}\Delta z_{0i}\frac{\partial^2 \phi}{\partial y \partial z}, \qquad i = 1, ..., n \end{aligned} \tag{20}$$

Finally, the discrete filter weights, w_i, can be evaluated from the first row of the pseudoinverse matrix A^+. Then, $\overline{\phi_0}$ can be written in terms of ϕ_i. So, at the end, it is possible to evaluate the least-squares reconstruction filter like any other standard convolution filter,

$$\overline{\phi_0} = \sum_{i=1}^{n} w_i \phi_i \tag{21}$$

or more algebraically,

$$\overline{\boldsymbol{\phi}} = \mathcal{F}\boldsymbol{\phi} \tag{22}$$

where $\mathcal{F}$ is the filter matrix, $\boldsymbol{\phi}$ the original scalar field, and $\overline{\boldsymbol{\phi}}$ the filtred field. Thus, to evaluate the filtred field only a matrix-vector product is needed (see Eqn. 22). Note, that the evaluation of the filter weights, w_i, is a preprocessing step, thus, there is no need to consern about the computational time required to solve the pdeudoinverse matrix.

The least-squares reconstruction filter generated by Haselbacher et al. methodollogy, conserves the commutative property but, unfortunately, it is not a self-adjont filter. That is, the filter it is not simetric. Thus, it is not a good cadidate to be used in conjuntion with the $\mathcal{C}_q$-regularization approximation, since the skew-symetric property of the convective operator may be loosed. A posible solution to this problem, is to force numerically the properties descrived in the Eqn 14 and 15. This can be easily achived, since the symmetry of the filter matrix can be forced algebraically,

$$\mathcal{F}_{sym} = \frac{1}{2}(\mathcal{F}^*\mathcal{F}) \tag{23}$$

And the normalisation of $\mathcal{F}_{sym}$ can be forced altering its diagonal.

In order to test the least-squares reconstruction filter (LSRF) and its symmetrical variant (Symmetric LSRF), a MMS study have been carried out. The ANSYS ICEM CFD package has been used to randomly generate 500 unstructured grids, in a hexahedrical domain, with tetrahedrical elements of a minimum aspect ratio of 0.3. The selected average mesh size, h, goes from $0.02L$ up to $0.5L$ (where L is a side of the hexahedrical domain). On each of these meshes the truncation error on the filtering stage have been evaluated for the two filters, i.e. $E = \| \overline{\phi_{ref}} - \overline{\phi} \|_\infty$(being $\overline{\phi_{ref}}$ the analytical result). In Figure 3, the truncation error is plotted versus the average mesh size. The solid lines are the least-squares fit to the points and have slopes of 3.09 for LSRF and 1.67 for the Symmetric LSRF.

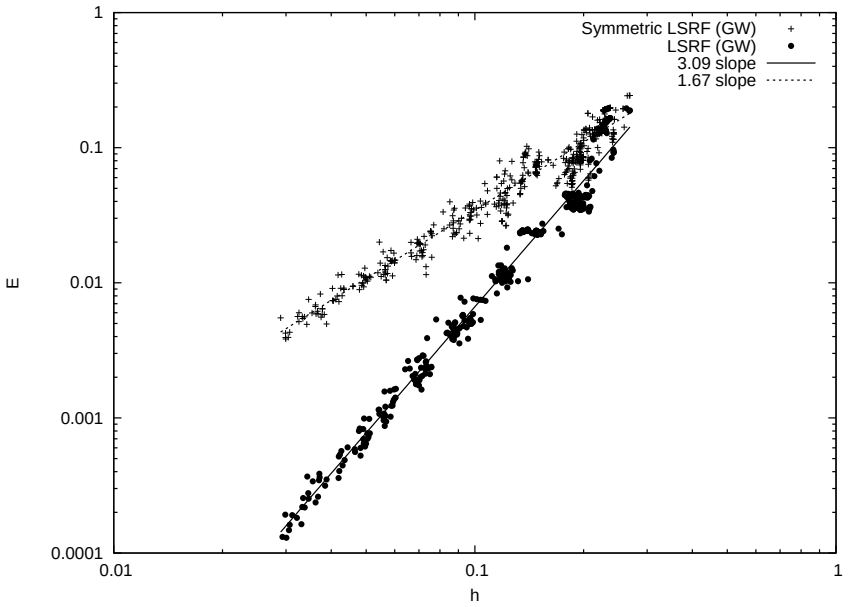

Figure 1: Truncation error, $E = \| \overline{\phi_{ref}} - \overline{\phi} \|_\infty$, versus average mesh size, for the LSRF and the Symmetric LSRF. Results are plotted in a log-log scale.

Evaluating the order of accuracy of both filters, it is clear that the Symmetric LSRF is not working as expected. This behaviour may be related with the aforementioned method to force the symmetry of the filter, where the symmetry of the filter matrix is forced *a-posteriori*. Unfortunately, this global operation breaks all the local properties of the original LSRF filter (note that the original LSRF has an approximate order of accuracy of 3). As a conclusion, our study has shown that is not posible to build an

accurate symmetric filter using Taylor series, i.e minimising the local truncation and commutative errors. The problem is, that the commutative property is juxtaposed to the property of symmetry, the first one is a local relationship and the latter is a global property. Thus, is difficult to change a filter so focused at the local character of the commutative property like the LSRF, in order to became symmetric. It is more advisable to seek a filter that takes this two properties as a whole from the scratch. Futhermore, the symmetry property seems to be more important than the commutative property in the $\mathcal{C}_q$-regularization context. Thus, in this work, both LSRF and its symmetric version will not be used, the first one, because it is not symmetrical and the second one by its lack of precision.

Another class of well-known LES filters are the differential filters[10]. These filters can be used under unstructured meshes, and they are by definition symmetric filters. Two of them are used in this work: a differential Helmholtz filter and a second order Gaussian filter. The first one is based on the elliptic differential operator:

$$\mathcal{F}^{-1}\overline{\boldsymbol{u}_c} = (\mathsf{I} - \alpha_k^2 \mathsf{L}_c)\overline{\boldsymbol{u}_c} = \boldsymbol{u}_c \tag{24}$$

where $\mathcal{F}^{-1}$ is the inverse of the transfer function of the filter. Fixing α_k as an isotropic case ($\alpha_k = \alpha$), Eqn. (24), becomes the inverse operator of the differential (or Helmholtz) filter, proposed by Germano[1].

The second filter is a non-uniform Laplace filter based on a Gaussian filter, which is always self-adjoint. The second term in the Taylor expansion of $\mathcal{F}\boldsymbol{u}$ for a Gaussian convolution filter is the Laplace operator[1]:

$$\mathcal{F}\boldsymbol{u}_c = (\mathsf{I} + \frac{\epsilon^2}{24}\mathsf{L}_c)\boldsymbol{u}_c = \overline{\boldsymbol{u}_c} \tag{25}$$

These filters are normalised conservative and also self-adjoint but the commutation property is not guaranteed (for general meshes). Notice that both, the elliptic filter and the Gaussian filter, are discretised in an identical manner than the diffusive term in Navier-Stokes equations. In both filters, the grid cutting length is evaluated using Deardorff's proposal[1]. This method is the most widely used today. It consists of evaluating the cutoff length as the cube root of the volume Ω of the filtering cell. Introducing the ratio $e = \epsilon/l$, where ϵ is the filter cutoff length and l is the grid cutting length.

4 NUMERICAL EXAMPLES

4.1 Numerical Method

The governing equations have been discretised on a collocated unstructured grid arrangement, by means of second-order spectro-consistent schemes[11]. Such discretisation preserves the symmetry properties of the continuous differential operators, i.e., the conservation properties are held if, the convective term is discretised by a skew-symmetric

operator and the diffusive term is approximated by a symmetric, positive-definite coefficient matrix. These properties ensure both, stability and conservation of the global kinetic-energy balance on any grid. An explicit third-order Gear-like scheme[12] based on a fractional step method is used for time-advancement algorithm, except for the pressure gradient where a first-order backward Euler scheme is used.

Collocated meshes do not conserve kinetic energy when fractional step method is used[13,14]. The source of these errors are interpolation schemes and inconsistency in the pressure field, in order to ensure mass conservation. While the first is eliminated through the use of consevative schemes, the latter equals to $\epsilon_{ke} = (\tilde{\boldsymbol{p}}_c)^* \mathsf{M}_c(\mathsf{G}_c - \mathsf{G}_s)\tilde{\boldsymbol{p}}_c$. Felten and Lund[14] showed that pressure errors are of the order of $\mathcal{O}(\triangle x^2 \triangle t)$. However, these errors do not have significant impact on the grid resolutions and time-steps used in LES and DNS.

4.2 Impinging Jet Flow at $Re_B = 20000$

Turbulent impinging jets have been the subject of many experimental research works[15,16]. However, they have been less studied by numerical simulations of the DNS or LES type[17]. The ability of the above presented regularization methodology is investigated to predict the overall field quantities in the plane turbulent impinging jet of aspect ratio $H/B = 4$ (where H and B are the height and the nozzle width respectively, see figure 2) with a moderate Reynolds number of 2×10^4.

The computational domain is a rectangular box of dimensions $L_x \times H \times L_z$ (see figure 2). The nozzle is centered in the upper bounday of the computational domain. The inlet vertical velocity (U_{ref}) is obtained from the Reynolds number value. No-slip condition is imposed at solid walls. At the exit boundary, a pressure-based boundary condition is used. Periodic boundary condition is used in the spanwise direction. In order to evaluate the accuracy of the symmetry-preserving formulation, two different grids are used. Considering the geometry of the computational domain, an hexahedral unstructured mesh is used, being more concentrated in the region near the impingement wall and coarse toward the exit and the center of the channel. The first one is a coarse grid (m1) of 11136 CVs and the second one a medium sized grid (m2) of 94080 CVs.

The numerical predictions of the mean flow and fluctuation quantities are compared with experimental data from Ashforth-Frost et al.[15] and Zhe and Modi[16]. All the results here presented have been obtained using the Helmholtz filter. However, the same study (not shown here) with the Gaussian filter has been also carried out. In addition, it has also been observed, that there is no influence in the results for a filter ratio $e > 3$. In Figure 3(a), streamwise velocity at three different locations in the impingement plate is plotted together with experimental data. As can be observed, very good agreement is obtained between numerical results using m2 mesh and experimental data. In fact, even for the simulation with the coarse mesh the results are reasonably good.

In addition to the mean flow features, the variation of the flow is important and the Reynolds stresses are mostly used to quantify the fluctuations of the flow. In Figure

3(b) comparison of streamwise velocity fluctuations u_{rms}/U_{ref} at the same locations in the impingement plate between the two meshes and the experimental data is shown. There is also a quite good agreement with experimental data for the m2 grid. This mesh is capable of fully describe the velocity fluctuations profile, except the peak in the stresses in the region close to the stagnation point where this quantity is slightly overpredicted. In general, the results obtained with this mesh are within the error range of both experimental studies. However, major discrepancies are obtained with the coarse grid. These differences are the largest in the region close to the impingement wall, where the coarse grid fails in the prediction of the peak in the turbulent intensities.

Based on the foregoing, regularization model seems to perform quite well for this kind of turbulent flows and on hexahedral grids. For a relative coarse grid of 94080 CVs, it is capable of reproducing the mean flow and its fluctuations within experimental accuracy.

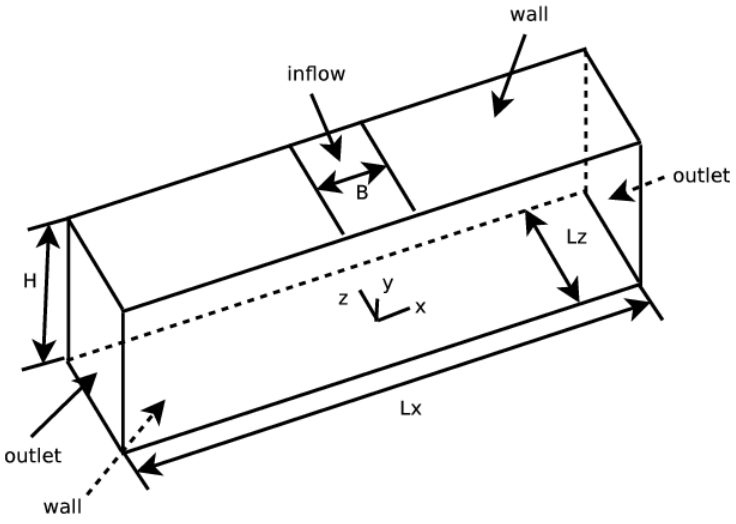

Figure 2: Impinging jet geometry

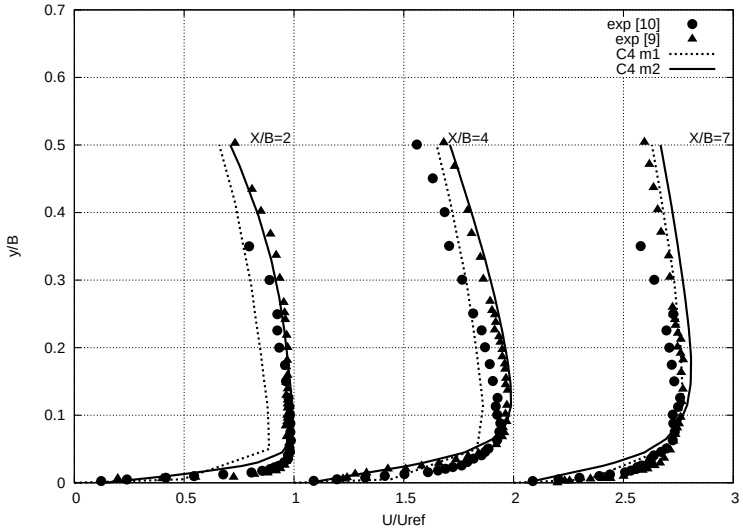

(a)

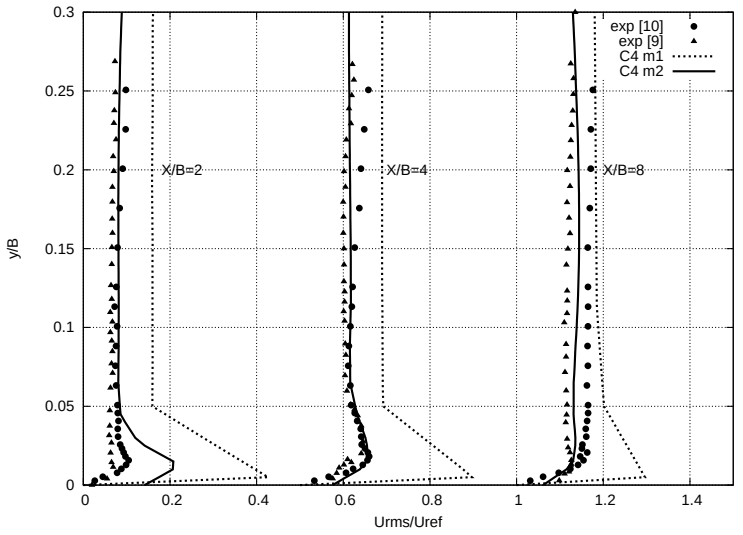

(b)

Figure 3: Streamwise velocity (a) and Reynolds stresses (b) at three different locations in the impingement plate. Lines: numerical solutions using two meshes; symbols: experimental data from Ashforth-Frost et al.[15] and Zhe and Modi[16].

4.3 Flow Around a Circular Cylinder at $Re_D = 3900$

As it is well known from experimental observations, the flow around a cylinder exhibits different behaviours depending on the Reynolds number[18]. At relatively high Reynolds numbers, the laminar to turbulent flow transition is not induced by the geometrical topology but due to instabilities in the separated shear layers. The unstable regions of the flow (where the turbulence is generated) can be roughly divided into three different zones: the boundary layer on the cylinder, the two shear layers, and the wake. In this section, attention is focussed on the flow at Reynolds number 3900 (defined in terms of the cylinder diameter D and free-stream velocity U_{ref}).

Numerical solutions have been obtained in a rectangurar computational domain of dimensions $x = [-4D, 20D]$, $y = [-8D, 8D]$, $z = [0, L_z]$ with a circular cylinder located at (0,0,0). A spanwise length of $L_z = \pi D$ has been considered in this study. The boundary conditions at the inflow consist of a uniform velocity, $(u, v, w) = (1, 0, 0)$. At top and bottom walls, symmetry boundary conditions are imposed. At the outlet boundary, pressure based condition is imposed. Periodic boundary conditions are used for the spanwise direction, being this direction Fourier transformed. No-slip conditions on the cylinder surface are set. The computational mesh used is an unstructured grid with prisms of 349408 CV. The use of the unstructured grid has allowed to cluster more control volumes near the circular cylinder boundary layer, in the shear layers and in the near wake.

In order to test the regularization modeling on general unstructured meshes, two different simulations have been performed. The first one using the Gaussian filter (see Eqn. 25) with a filter ratio $e = 1$, and the second one using the Helmholtz filter (see Eqn. 24) with a filter ratio $e = 4$. At this point, it is important to remark that the stability of the Gaussian filter is restricted by the filter ratio. On the contrary, the Helmholtz filter seems to be less dependent of the filter ratio. This is the reason for the lower value of the filter ratio used for the Gaussian filter.

Numerical results obtained with the two filters in comparison with reference data from DNS[19] are given in figure 4. In the figure, the streamwise and cross-flow velocities profiles of the time-average flow at three different locations in the wake of the circular cylinder are plotted (see figures 4(a) and 4(c)). Turbulence intensities $< u'u' > /U_{ref}$ and $< v'v' > /U_{ref}$ for $x/D = 1.54$ are also depicted (figures 4(b) and 4(d)). The mean flow solution obtained with the Helmholtz filter is in very good agreement with the reference data from DNS. Although the simulation using the Gaussian filter does not perform inadequately, the results obtained seems to be in worst agreement than those with the Helmholtz filter.

Regarding to second-order statistics, the simulation using the Helmholtz filter are in correspondence with the reference data, predicting very well the peak in the stresses. On the other hand, the Gaussian filter are less satisfactory and although it predicts the shape of the Reynolds stresses curves and the position of the peak in the stresses, clearly under-predict their magnitude.

As a conclusion, the solution obtained with the Regularisation model seems to be

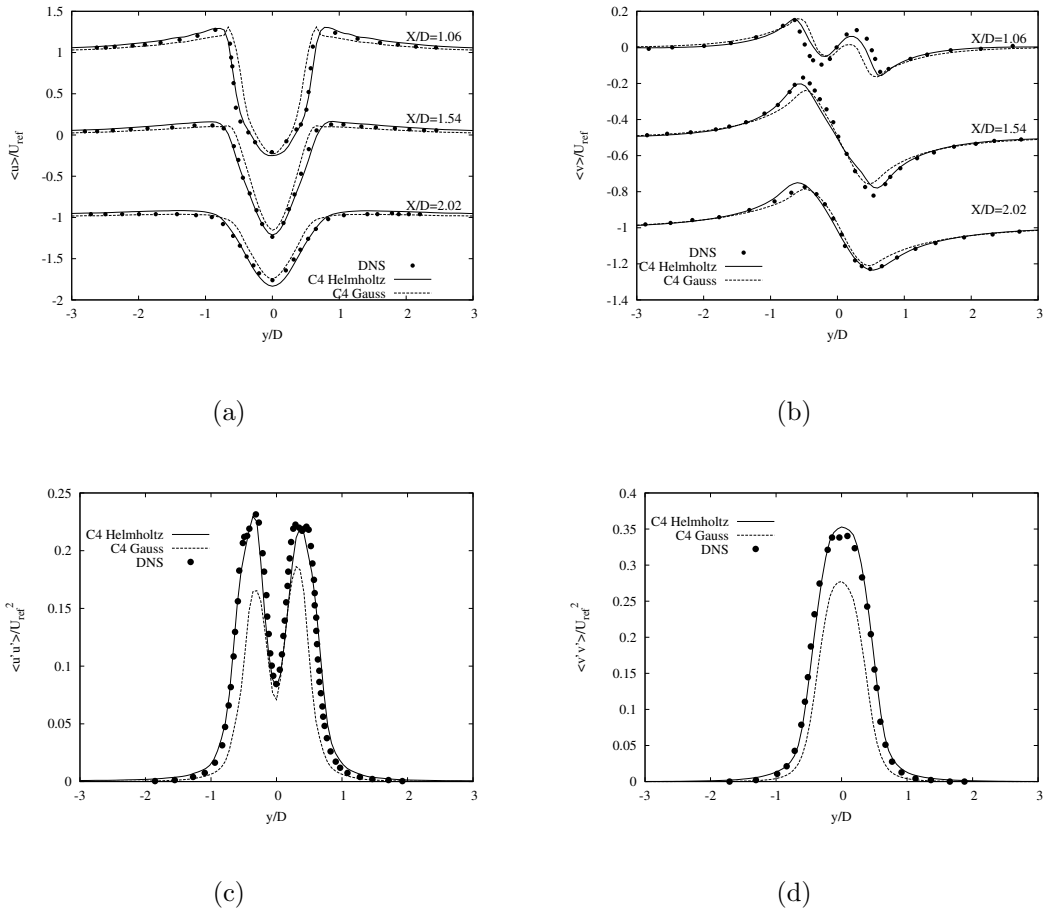

Figure 4: Results obtained at three locations in the wake of a circular cylinder. Comparison with DNS [19] data. (a) Streamwise velocity $< u > /U_{ref}$, (b) cross-flow velocity $< v > /U_{ref}$, (c) streamwise velocity fluctuations $< u'u' > /U_{ref}^2$ and (d) cross-flow velocity fluctuations $< v'v' > /U_{ref}^2$.

affected by the performance of the filter. In this case, the simulation using Helmholtz filter is quite better good agreement with DNS data than the one obtained with the Gaussian filter. Moreover, the results with the Helmholtz filter are excellent taking into account that traditionally LES of this case have been solved using meshes of 1.5-2.5 million CVs. For example, the numerical studies by Kravchenko and Moin [20] were performed using 1.5 million CVs and a conventional dynamic LES model.

4.4 Turbulent flow over an Ahmed car at $Re = 7.68 \cdot 10^5$

The Ahmed body car is a semi-rectangular vehicle with a rounded front part and a slant back. Flow over this generic body reproduce the basic fluido-dynamics features of real cars with a typical fastback geometry and its simplified topology allows easy comparisons

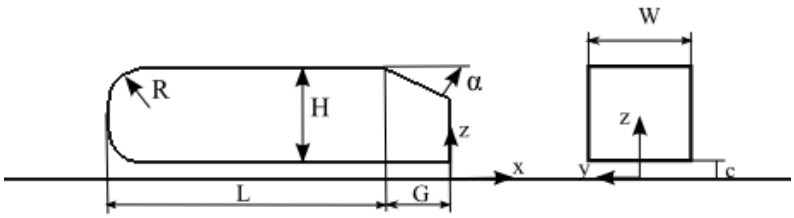

Figure 5: Ahmed body car geometry

between experimental and numerical works.

Ahmed *et al.*[21] have carried out experiments of this vehicle with several slant angles (α) and described the characteristics of the flow for various angles. Their conclusions were that the flow is fully unsteady, three-dimensional and shows separations than can be followed by reattachments depending on α. The flow also shows large unsteady phenomena coming from interactions between recirculation bubbles and vortices. Moreover, a critical $\alpha \sim 30^o$ was found to lead an abrupt decrease in drag associated with the merging of separation regions and vortex breakdown. This test case was selected for the 9^{th} ERCOFTAC Workshop since the complex features of the flow make computations a challenging task, from both, the modeling and the numerical point of view. It was concluded that the unsteady simulation methods like URANS and LES have a stronger potential to accurate capture the details of the flow than the standard RANS techniques, but the case was still not considered to be satisfactory predicted for the subcritical angle ($\alpha = 25^o$).

All these difficulties are mainly related to the partial deattachment of the flow at the beginning of the slant. As Krajnovic *et al.*[22] have proved the shear related to the small-scale structures generated by the deattachment significantly increases the turbulent stresses. Also, experimental measurements by Lienhart *et al.*[23] shown that at the slant mixing layer, the turbulent kinetic energy is much higher than in the canonical self-similar mixing cases.

We have selected this case to study the performance of the Regularization modeling on complex flows. The geometry has been defined as in the experiments of Ahmed *et al.*[21] (see figure 5). The values of the body heigth is $H = 0.288m$. The other geometric values are $L_r = 0.8428m$, $G = 0.2012m$, $W = 0.389m$ and $C = 0.05m$. The slant angle considered is $\alpha = 25°$. The comoputational domain considered is a rectangular channel of dimensions $9.1944 \times 1.87 \times 1.4$, with the front of the body located at a distance from the inlet of 2.1024m. The downstream region has a length of 6.048m measured from the rear end of the car. The Reynolds number based on the inlet velocity, U_red, and the car heigth, H, is of $Re = 7.68 \times 10^5$. At the inflow, uniform axial velocity profile is imposed. At the lateral and top walls, slip boundary conditions are prescribed. At the outflow of the domain, a pressure-based boundary condition is applied. In addition, a buffer zone

is defined at $x > 5$, in order to suppress non-physical waves which are reflected by the outflow boundary. No-slip conditions at the bottom surface are considered.

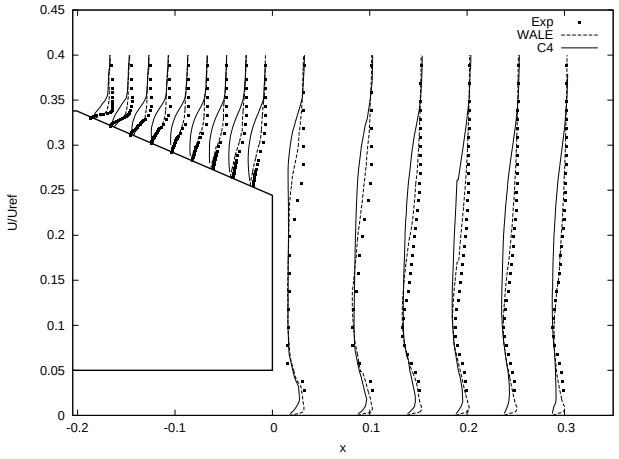

Figure 6: Mean streamwise velocity profiles in the symmetry plane: solid line C4, dashed line WALE model, dots experiments[23]

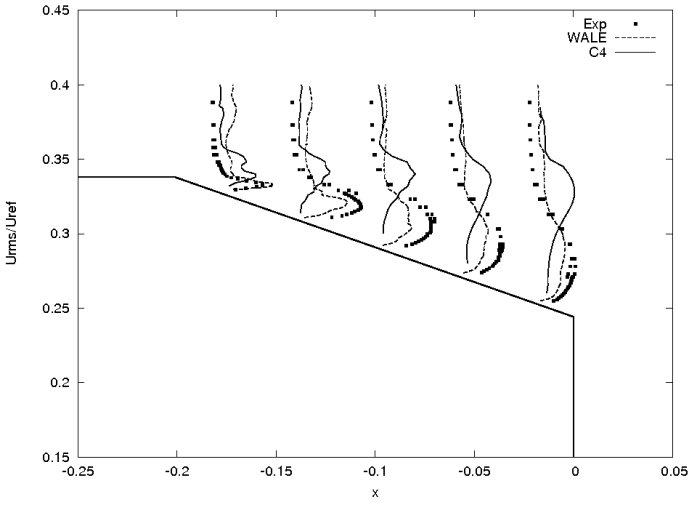

Figure 7: Root mean square of the streamwise velocity fluctuationsu_{rms} profiles in the symmetry plane: solid line C4, dashed line WALE model, dots experiments[23]

The calculations have been performed on an hybrid prism-hexahedral unstructured grid of 662282 CVs. A prism-layer to capture the body boundary layer is constructed around the car surface. Results obtained have been compared with the experimental data of

Leinhart *et al.*[23] and also with numerical results obatined using Large Eddy Simulations with the wall adapting local eddy viscosity (WALE)[5] model for the subgrid scale stresses.

In figure 6 the mean streamwise profiles of the velocity for the symmetry plane ($y = 0$) at the rear end of the body and at the near wake are shown. As can be seen, there are significant differences concerning the prediction of the mean flow behaviour in the slant back. In our results with the regularization model, the flow separates in the slant corner and forms a large recirculation zone. Furthermore, the flow does not reattaches the slant as in the experiments. Although, *a-priori* it is possible to attribute this behaviour to a poor resolution near the wall, when comparing with the performance of the WALE model on the same grid, it can be observed that the WALE model shows a quite good agreement with the experiments even for this coarse grid. As expected, larger discrepancies are obtained in the prediction of the Reynolds stresses as can be seen in figure 7. In this case, the performance of the model is strongly affected by the filtering quality. This is more important in the zone of the slant near the wall, where the mesh is an hybrid between prism and tetrahedral control volumes.

5 CONCLUSIONS

In this paper an assessment of regularization models on unstructured meshes has been presented. As a first step, the symmetry-preserving regularization turbulence modelling has been described, paying special attention to the different filters to be used. In order to analyse the influence of the filter on the modeling, a detailed study of the properties of standard filters for unstructured grids has also been done. Finally, using this modeling, three different test cases have been studied: the impinging jet flow, the flow past a circular cylinder and a simplified Ahmed car. Furthermore, the performance of the model considering the influence of the grid parameters and the filter ratio have been also analysed.

It has been shown, the filters based on least-squares minimization procedures are not suitable for regularization models since they are not symmetrical. On the other hand, differential filters are a better alternative because they are symmetrical by construction. Our numerical test shows that when structured meshes or smooth unstructured meshes are used, this kind of filters are very efective. As a proof of this statement, some results for an impinging jet and the flow over a circular cylinder have been presented. Taking into account traditionally LES results for the same type flow our $\mathcal{C}_4$ simulations are excellent. Thus, $\mathcal{C}_q$-regularization modeling seems to be an accurate approximation of the Navier-Stokes equations even on complex flows.

Finally the flow over an Ahmed car have been selected to test the behaviour of the aforementioned methodology under fully irregular unstructed grids. Here, the obtained results had significant differences concerning the prediction of the mean flow behaviour in the slant back of the car. Our conclusion is that in this case the performance of the model is strongly affected by the filtering quality. This is more relevant in the zone of the slant near the wall, where the mesh is an hybrid between prism and tetrahedral control

volumes. In this zone the mesh rarely satisfy smoothness constrains on the grid spacing. Since the used differential filter has been discretised in an identical manner than the difusive term in Navier-Stokes equations it can be argued that the filter truncation errors are afecting the high-frequency components of the discrete filtered velocity vector. Thus, to avoid such numerical interaction between the filter and the modeled scales it may be interesting to discretise the differential filter with high order scheme. This aspect will be studied in future works. Another posible solution may be the use of power of Laplacian filters as Trias and Verstappen have recently pointed out[24].

ACKNOWLEDGEMENTS

This work has been by financially supported by the Ministerio de Educación y Ciencia, Secretaría de Estado de Universidades e Investigación, Spain (ref. ENE2009-07689) and by the Collaboration Project between Universidad Politècnica de Catalunya and Termo Fluids S.L. (ref. C06650)

References

[1] P. Sagaut. *Large Eddy Simulation for Incompressible Flows*. Springer-Verlag, 2001.

[2] Stephen B. Pope. *Turbulent Flows*. Cambridge University Press, 2000.

[3] David C. Wilcox. *Turbulence Modeling for CFD*. DCW Industries, Inc. La Caada, California, 1993.

[4] T.J.R. Hughes, L. Mazzei, and K.E. Jansen. Large eddy simulation and the variational multiscale method. *Computing and Visualization in Science*, 3:47–59, 2000.

[5] F. Nicoud and F. Ducros. Subgrid-Scale Stress Modelling Based on the Square of the Velocity Gradient Tensor. *Flow, Turbulence and Combustion*, 62:183–200, 1999.

[6] B. J. Geurts and D. D. Holm. Regularizarition modeling for large-eddy simulation. *Physics of Fluids*, 15:L13–L16, 2003.

[7] J. Leray. Sur le movement d'un liquide visqueaux emplissant l'espace. *Acta Mathematica*, 63:193–248, 1934.

[8] Roel Verstappen. On restraining the production of small scales of motion in a turbulent channel flow. *Computers and Fluids*, Vol. 37(7):887–897, 2008.

[9] A. Haselbacher and O. V. Vasilyev. Commutative discrete filtering on unstructured grids based on least-squares techniques. *Journal of Computational Physics*, 187:197–211, 2003.

[10] M. Germano. Differental filters for large eddy numerical simulation of turbulent flows. *Physics of Fluids*, 29(6):1755–1758, 1986.

[11] R. W. C. P. Verstappen and A. E. P. Veldman. Symmetry-Preserving Discretization of Turbulent Flow. *Journal of Computational Physics*, 187:343–368, May 2003.

[12] G.M. Fishpool and M.A. Leschziner. Stability bounds for explicit fractional-step schemes for the Navier-Stokes equations at high Reynolds number. *Computers and Fluids*, 38:1289–1298, 2009.

[13] Y. Morinishi, T.S. Lund, O.V. Vasilyev, and P. Moin. Fully conservative higher order finite difference schemes for incompressible flow. *Journal of Computational Physics*, 143(1):90–124, 1998.

[14] F.N. Felten and T.S. Lund. Kinetic energy conservation issues associated with the collocated mesh scheme for incompressible flow. *Journal of Computational Physics*, 215(2):465–484, 2006.

[15] S. Ashforth-Frost, K. Jambunathan, and C. F. Whitney. Velocity and Turbulence Characteristics of a Semiconfined Orthogonally Impinging. *Exp. Thermal and Fluid Science*, 14:60–67, 1997.

[16] J. Zhe and V. Modi. Near Wall Measurements for a Turbulent Impinging Slot Jet. *Journal of Fluids Enginnering*, 123:112–120, 2001.

[17] H. Hattori and Y. Nagano. Direct numerical simulation of the turbulent heat transfer in plane impinging jet. *International Journal of Heat and Fluid Flow*, 25(5), 2004.

[18] A. Prasad and C. H. K. Williamson. The instability of the separated shear layer from a bluff body. *Phys. Fluids*, 8:1347, 1996.

[19] O. Lehmkuhl, R. Borrell, C. D. Pérez-Segarra, J. Chiva, and A. Oliva. Direct Numerical Simulations and Symmetry-Preserving Regularization Simulations of the flow around a circular cylinder at Reynolds number 3900. In *Turbulence, Heat and Mass Transfer 6*, Rome, Italy, September 2009.

[20] A. G. Kravchenko and P. Moin. Numerical studies of flow over a circular cylinder at $Re_D = 3900$. *Physic of Fluids*, 12:403–417, 2000.

[21] S. R. Ahmed, G. Ramm, and G. Faltin. Salient features of the time-averaged ground vehicle wake. *SAE Paper*, (840300), 1984.

[22] S. Krajnović and L. Davidson. Flow Around a Simplified Car, Part 1: Large Eddy Simulation. *Journal of Fluids Engineering*, 127:907–918, 2005.

[23] H. Lienhart and S. Becker. Flow and Turbulent Structure in the Wake of a Simplified Car Model. *SAE Paper*, (2003-01-0656), 2003.

[24] F.X.Trias and R.W.C.P.Verstappen. On the construction of discrete filters for symmetry-preserving regularization models. *Computers and Fluids*, (submitted).